Breakage and Attrition of Sintered Agglomerates

S. Luding

(1) Institut für Computerphysik, Universität Stuttgart, Pfaffenwaldring 27, 70569 Stuttgart, Germany
(2) Particle Technology, Nanostructured Materials, DelftChemTech, TU Delft, Julianalaan 136, 2628 BL Delft, The Netherlands
e-mail: s.luding@tudelft.nl

Abstract. A model for the sintering of polydisperse, inhomogeneous arrays of cylinders is presented with empirical contact force-laws, taking into account plastic deformations, adhesion, temperature dependence (melting), and long-time effects. Samples are prepared under constant isotropic load, and are sintered for different sintering times. Increasing both external load and sintering time leads to a stronger, stiffer sample after cooling down. The material behavior is interpreted from both microscopic and macroscopic points of view. Compression and vibration tests lead to breakage and attrition, respectively. Among the interesting results is the observation, that the coordination number, even though it has the tendency to increase, sometimes slightly decreases, whereas the density continuously increases during sintering – this is interpreted as an indicator of reorganization effects in the packing. Another result of this study is the finding, that strongly attractive contacts occur during cool-down of the sample and leave a sintered block of material with almost equally strong attractive and repulsive contact forces.

1. Introduction

In mechanics and physics there are two ways to model a particulate, inhomogeneous material like powder-ceramics. The first approach is based on continuum theory and relies on empirical assumptions about the macroscopic material behavior, [1, 2, 3, 4, 5, 6, 7, 8, 9] . The macroscopic approach can be complemented by a more "microscopic" description of the material on the particle or grain level, where the particles and their interaction dynamics are modeled explicitly [10, 11, 12, 13]. The former involves stress, strain and plastic yield conditions [14], whereas the latter deals with local force-deformation laws for each contact [15]. The macroscopic approach neglects the microstructure due to its nature and often wrong assumptions, e.g., about isotropy are made.

In the following, certain contact force-laws are proposed and we will restrict ourselves to two dimensions. A clear disadvantage of discrete models is the limited number of particles that can be modeled with reasonable effort. Therefore, rather than examining large structures, we focus on small samples with a few hundred particles only. Different sintering times and confining pressures will lead to different agglomerate strengths.

2. Model System

Because it is rather difficult to observe what is going on inside the material during an experiment, the alternative simulations with the discrete element model (DEM) is applied here [10, 16, 17]. The numerical "experiment" chosen is a bi-axial box set-up, as described in [12], where the left and bottom walls are fixed, and a stress-control is applied to the other walls. Three forces are active: (i) the force due to the bulk material, (ii) the force due to the external pressure, and (iii) a viscous force which damps the motion of the wall so that oscillations are reduced.

Inside the system, N disks with radii a_i ($i = 1, \ldots, N$) and height h are placed. The radii are drawn from a homogeneous distribution with mean a_0 and relative width w_0 so that $a_i/a_0 \in [1-w_0, 1+w_0]$. The particle-particle interactions and the parameters involved are discussed in the next section.

3. Discrete Particle Model

Since the realistic modeling of the deformations of the particles is much too complicated to allow for a subsequent many-particle simulation, the interaction force is related to the overlap δ of two particles. In the absence of long-range forces (as assumed in this study), an interaction takes place only if particles are in contact and thus $\delta > 0$. The forces are split into a normal and a tangential component denoted by indices n and t, respectively. Note that for varying temperature, the particle radius is changing so that the inhomogeneous structure implies changes of overlap conditions and thus of forces

– only due to a temperature change. If all forces $\boldsymbol{f}_i$ acting on the particle i, either from other particles, from boundaries or from external forces, are known, the problem is reduced to the integration of Newton's equations of motion for the translational and rotational degrees of freedom [12].

3.1. Normal Contact Model

Two particles i and j at positions $\boldsymbol{r}_i$ and $\boldsymbol{r}_j$, with radii a_i and a_j, interact only if they are in contact so that their overlap

$$\delta = (a_i + a_j) - (\boldsymbol{r}_i - \boldsymbol{r}_j) \cdot \boldsymbol{n} \tag{1}$$

is positive, with the unit vector $\boldsymbol{n} = \boldsymbol{n}_{ij} = (\boldsymbol{r}_i - \boldsymbol{r}_j)/|\boldsymbol{r}_i - \boldsymbol{r}_j|$ pointing from j to i. The force on particle i, from particle j can be written as $\boldsymbol{f}_{ij} = f_{ij}^n \boldsymbol{n} + f_{ij}^t \boldsymbol{t}$, with $\boldsymbol{n}$ perpendicular to $\boldsymbol{t}$. In this subsection, the normal forces are discussed.

3.1.1. Short time contact model First, the time- and temperature-independent behavior of the contact forces between a pair of particles is discussed. For this, we modify and extend the linear hysteretic spring model [12, 18, 19, 20, 21], which contains elastic repulsion, plastic contact deformation and adhesion:

$$f_{ij} = \begin{cases} k_1 \delta & \text{loading,} \\ k_2(\delta - \delta_0) & \text{un/reloading,} \\ -k_c \delta & \text{unloading,} \end{cases} \tag{2}$$

with $k_1 \leq k_2$, see Fig. 1, and k_c determining the magnitude of adhesion, i.e., the maximal attractive force, $f_{\min}$. For a detailed description of this model, see Ref. [12].

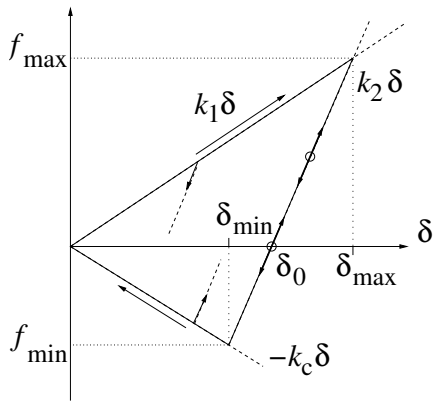

Figure 1. Force law for two springs with stiffness k_1 and k_2 for initial loading and subsequent un/reloading, respectively. Attractive forces are possible due to the adhesion strength k_c.

The cone formed by the lines with slope k_1 and $-k_c$ defines the range of possible force values. If a force would fall outside the cone, it is forced to remain on the limit lines. Departure from these lines into the cone takes place in the case of unloading and

reloading, respectively. Between these two extremes, unloading and reloading follow the same line with slope k_2. Different maximal overlaps imply different stiffness k_2, however.

3.1.2. Viscous dissipation For small displacements around some equilibrium state, the model does not contain dissipation. In order to allow for stronger dissipation and thus faster relaxation, a viscous, velocity dependent dissipative force in normal direction,

$$f_{ij}^{n,\mathrm{d}} = \gamma_0 \dot{\delta} \ , \tag{3}$$

is assumed with some damping coefficient γ_0. This leads to, see [19], a contact duration (or inverse eigen-frequency) $t_c = \pi/\omega$, with $\omega = \sqrt{k_2/m_{12} - \eta_0^2}$, with the rescaled damping coefficient $\eta_0 = \gamma_0/(2m_{12})$, and the reduced mass $m_{12} = m_1 m_2/(m_1+m_2)$. The time-step of the simulations has to be chosen as $t_{\mathrm{MD}} \approx t_c/50$ for a proper integration of the equations of motion.

3.1.3. Stiffness increase with contact area In order to account for the fact that a larger contact surface leads to a larger contact stiffness, the coefficient k_2 is made dependent on the maximum overlap history parameter $\delta_{\max}$ (and thus on the force-free overlap δ_0), as long as the overlap is below the threshold δ^{fluid} that corresponds to the "complete melting" of the particles. Complete melting is here the limit of an incompressible liquid that is contained in the model, however, neither discussed in detail nor verified for reasons of brevity.

The stiffness is maximal in the fluid limit for $\delta_0 = \delta^{\mathrm{fluid}}$, which corresponds to $\delta_{\max} = \delta_{\max}^{\mathrm{fluid}} = k_2\delta^{\mathrm{fluid}}/(k_2 - k_1)$, and varies between k_1^0 and k_2 for smaller overlaps, so that

$$k_2(\delta_{\max}) = \begin{cases} k_2 & \text{if } \delta_{\max} \geq \delta_{\max}^{\mathrm{fluid}} \\ k_1^0 + (k_2 - k_1)\frac{\delta_{\max}}{\delta_{\max}^{\mathrm{fluid}}} & \text{if } \delta_{\max} < \delta_{\max}^{\mathrm{fluid}} \end{cases} \ . \tag{4}$$

For large overlaps (in the fluid regime), the stiffness and the force is thus only dependent on k_2, independent of k_1. For smaller overlaps k_1, k_1^0, and k_2 affect the force together with the history of this contact.

The hysteretic stiffness model thus takes into account an increasing stiffness with increasing deformation. The first loading is plastic with low stiffness, and subsequent un- and reloading are stiffer because the material was initially compressed. As a consequence, also the maximum adhesive force depends on the maximum compression which was experienced by the contact during its history.

3.2. Density Temperature Dependence

The temperature dependent density of the single particles, with the density change per unit temperature $\delta\rho_T$, leads to a particle radius

$$a(T) = a(T_{\mathrm{melt}})[1 - \delta a_T\,(T_{\mathrm{melt}} - T)] \ , \tag{5}$$

with the relative change of the radius per unit temperature δa_T. In the following, we use $\delta a_T = 10^{-4}\,\mathrm{K}^{-1}$, so that the particle radius is changed by 0.01 per-cent if the

temperature is changed by one Kelvin. Note however, that this is an arbitrary choice (reasonable for polyamid); coefficients for steel and glass are typically one and two orders of magnitude smaller, respectively.

3.3. Contact Temperature Dependence

For the temperature dependence, we focus on an inhomogeneous material with a typical melting temperature T_{melt}. The material behaves as described above, if the temperature T is much smaller than the melting temperature. For higher temperatures k_1 decreases and also the other material parameters are changed [12, 13].

When the temperature is increased to a rather large value, close to the melting point, two particles under stress and in equilibrium due to compressive forces will lose stiffness and thus will deform more strongly so that their overlap becomes larger:

$$k_1(T) = \frac{k_1}{2}\left[1 + \tanh\left(\frac{T_{\mathrm{melt}} - T}{T_{\mathrm{var}}}\right)\right] = \frac{k_1}{2}\left[1 + \tanh(\tau)\right] \ , \tag{6}$$

where τ denotes the ratio of the temperature difference to the range of considerable temperature dependency T_{var}. When k_1 is reduced due to an increase in temperature (+), we assume that δ^+_{max} remains constant, so that one obtains a larger force-free overlap $\delta^+_0(T) = [1 - k_1(T)/k_2(\delta^+_{\mathrm{max}})]\delta^+_{\mathrm{max}}$. Thus the material volume shrinks due to sintering at the contact level.

Note that k_2 is not changed directly when $k_1(T)$ is decreased, see the left panel in Fig. 2 or Eq. (4). The adhesion in this model, however, is directly affected by a change of $k_1(T)$, see Eq. (7) below. In a pre-stressed situation, corresponding to a finite confining force at the contact, also δ^+_{max} is shifted in order to balance the confining force – but only after $k_1\delta^+_{\mathrm{max}}$ became smaller than the confining force.

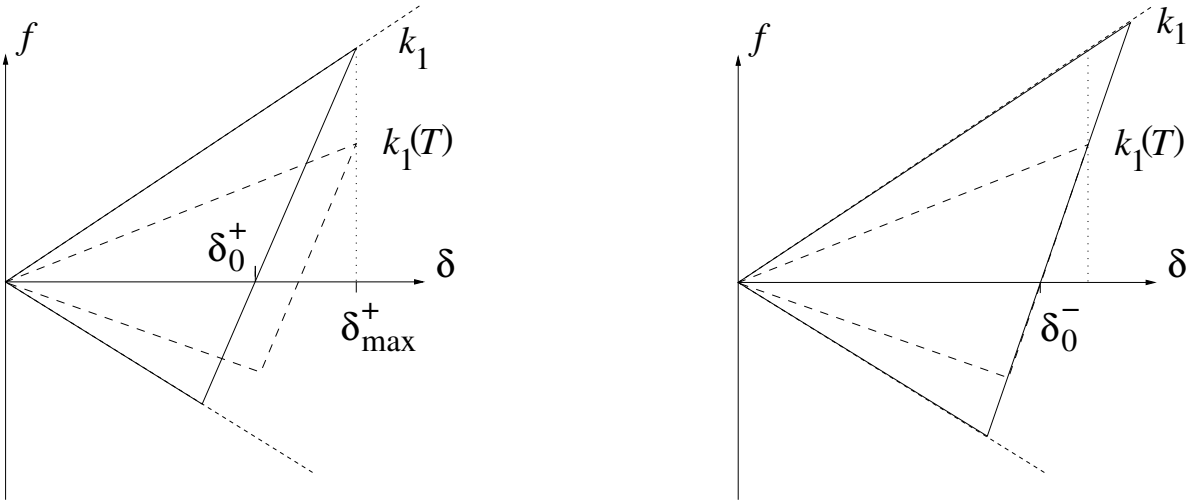

Figure 2. Force laws for varying stiffness k_1, according to Eq. (6). (Left) If the temperature is increased, k_1 is reduced while δ^+_{max} remains constant (dashed line, stress-free case). (Right) If the temperature is subsequently decreased, k_1 is increased while δ^-_0 remains constant (solid line with slope k_2).

If the temperature is decreased, $k_1(T)$ is adjusted according to Eq. (6), but since the melted (sintered) area around the contact point will not return to its previous overlap state, we assume $\delta_0^- = \text{const.}$, so that the maximum overlap increases to the value $\delta_{\max}^-(T) = \delta_0^-/[1 - k_1(T)/k_2]$, see the right panel in Fig. 2. During heating/cooling, the contact deformation/area and thus the force-free overlap can become larger due to the partial melting of the surface and also the stiffness is increased accordingly.

3.4. Temperature dependence with time

In the material there are several time dependent processes, like diffusion, taking place [23, 24]. We are interested in the slow, long time behavior of the material, we assume that heat conduction and equilibration take place instantaneously, as long as temperature changes are small and slow. The short time dynamics is translated into a delayed change of the material parameters above, see [12] for details. The changes of stiffness are faster for higher temperatures. In the hot limit, changes take place very rapidly, whereas in the cold limit changes are extremely slow. Note that the adaptation/relaxation of, e.g., $k_1(T,t)$ to the desired $k_1(T)$ value is not delayed when the temperature is decreasing and $k_1(T) > k_1(T,t)$. In that situation the contacts freeze rapidly and thus have to become strong as fast as the system cools down.

3.5. Adhesion dependence on stiffness

The adhesive properties of a particle contact depend on the temperature, in so far that a melted contact should have weak tensile and compressive strength. Therefore, we couple the adhesive parameter k_c to the magnitude of $k_1(T,t)$. In order to take into account a reduced tensile strength of a soft contact with weak deformation and thus small overlap, the adhesion is directly related to the stiffness:

$$k_c(T,t,\delta_{\max}) = \frac{k_1(T,t)}{k_1}\frac{k_2(\delta_{\max})}{k_2}k_c \ . \tag{7}$$

This is an arbitrary choice for the adhesion factor k_c, but as long as no detailed experimental results are available, we stick to this simple empirical assumption.

3.6. Tangential Contact Model

The force in the tangential direction is implemented in the spirit of Cundall and Strack [16] who introduced a tangential spring in order to account for static friction and elastic energy stored in the contact tangential direction. The detailed friction law is discussed in Ref. [12], so that we here only summarize the non-standard issues. The relevant normal force computed with respect to the minimal force $f_{\min}$ so that the tangential force becomes $f^t \leq \mu(f^n - f_{\min})$. Besides the combination of the adhesive and the frictional force, also the tangential dissipation is non-standard, as described in [12, 21, 22]. Furthermore, we remark that the adhesion could also be coupled to friction in the sense that a broken contact loses its tensile strength when it is assumed brittle, so

that $k_c = 0$, (if sliding), i.e. if one has a sliding contact with $f^t = \mu(f^n - f_{\min})$. On the other hand, if the particles are very small, attractive forces could still be present so that k_c would not be affected by the type of the contact being either sliding or sticking. In this study we assume, as an arbitrary, possibly inconsistent choice, $f^n \geq 0$, (if sliding), thus disregarding adhesion in the sliding situation. The effect of this choice has to be examined in more detailed elsewhere. All this is still open to discussion and experimental validation.

3.7. Temperature dependence in tangential direction

In parallel to the change of normal stiffness, the tangential stiffness is always kept in a constant ratio to k_2 so that

$$k_t = \alpha k_2(\delta_{\max}) \ , \tag{8}$$

since the stiffness in the tangential direction is based on the same arguments as the material stiffness in the normal direction.

The friction is coupled to the temperature dependent value of the stiffness $k_1(T, t)$, because friction should not be present in a liquid at large enough temperatures, so that

$$\mu(T, t) = \frac{k_1(T, t)}{k_1}\mu \ . \tag{9}$$

Thus friction is modified together with the changes in normal direction. No further new ideas are introduced for the tangential forces.

3.8. Contact torques and couples

The tangential sliding force leads to a torque and thus to rotations of the particles. In addition to the sliding friction force, as related to the relative displacement in tangential direction, also rolling resistance and contact normal torsion have to be implemented in a realistic three dimensional model.

4. Results

The sintering model is applied to the sintering process of a particulate material sample. The material is initially a loose powder and first has to be prepared at low temperature from time t_0 to time t_{heat}. The preparation takes place with isotropic external pressures $p := p_{\text{w}} = p_x = p_z = 10$ or 100. The particles are randomly placed in a box with random initial velocity. Then the walls compress the system and motion is dissipated until a quasi-static situation is reached. Here, we used frictionless particles for the initial compression and thus obtain an over-consolidated initial packing. The system parameters are described in detail in Ref. [12].

The initial relaxation takes place at constant temperature $T = 80^0$C until time t_{heat}, when the system is heated up to $T = 140^0$C between time t_{heat} and t_{sinter}. During the sintering time, t_s, the system is allowed to sinter. At the end of the sintering process,

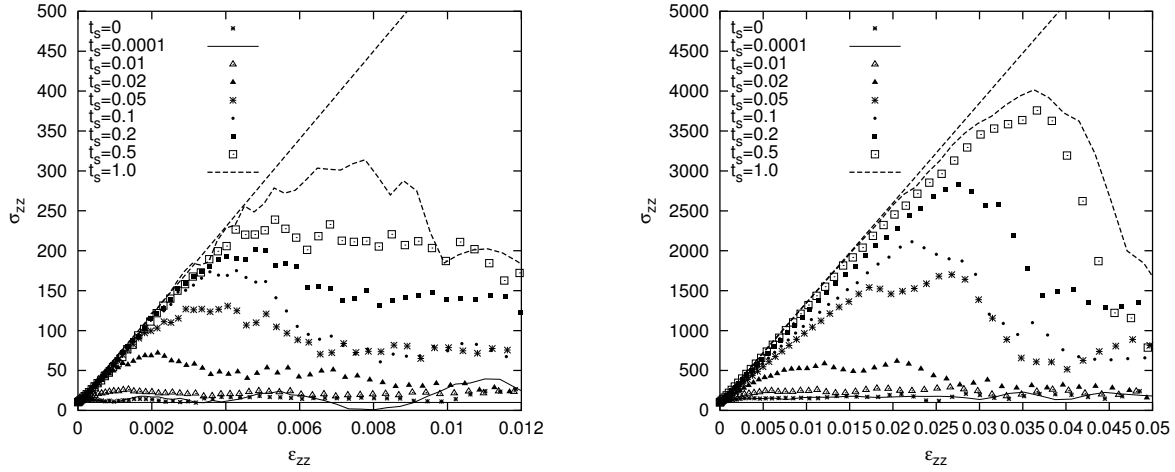

Figure 3. Vertical stress as function of the vertical strain for samples prepared with different sintering times t_s and different pressure $p_\mathrm{w} = 10$ (Left) and $p_\mathrm{w} = 100$ (Right). The slope of the dashed line (material stiffness) is about double for the higher pressure.

at time t_cool, the sample is slowly cooled down and, at time t_relax allowed to relax at constant temperature until time t_f. With this finished sample, tests will be performed.

For the preparation of the sample, we use the times $t_0 = 0$, $t_\mathrm{heat} = 0.2$, $t_\mathrm{sinter} - t_\mathrm{heat} = 0.1$, different sintering times $t_s := t_\mathrm{cool} - t_\mathrm{sinter}$, $t_\mathrm{relax} - t_\mathrm{cool} = 0.1$, and $t_\mathrm{f} - t_\mathrm{relax} = 0.1$.

In general, longer sintering and larger confining pressures lead to higher densities of the sintered sample. Through test simulations with different parameters, we verified that the increase in density is only partially due to the contact model, but also is caused by reorganizations in the sample. The thermal expansion of the particles, on the other hand, seems to be less important.

4.1. Compression test

For the compression test of the samples with 300 particles, the top wall is displaced slowly downwards with pre-defined vertical strain. The vertical stress is plotted against the strain in Fig. 3. With increasing strain, the vertical stress in the sample increases and it fails typically at some slightly larger strain and stress as compared with the small sample. The failure stress increases with increasing sintering time, increasing external stress, and also with increasing sample size. The material stiffness (dashed line in Fig. 3) is increasing by a factor of two when the confining stress is increased by a factor of ten. The critical strain where the material fails increases with increasing confining pressure, sintering time and system size.

4.2. Vibration test

Removing all side and top walls, the samples – due to gravity – collapse on the ground. A poorly sintered powder will form a heap, whereas a sintered block of material will keep

its identity. These sintered samples can be vibrated in order to probe their stability, breakage and attrition, see Figs. 4 and 5.

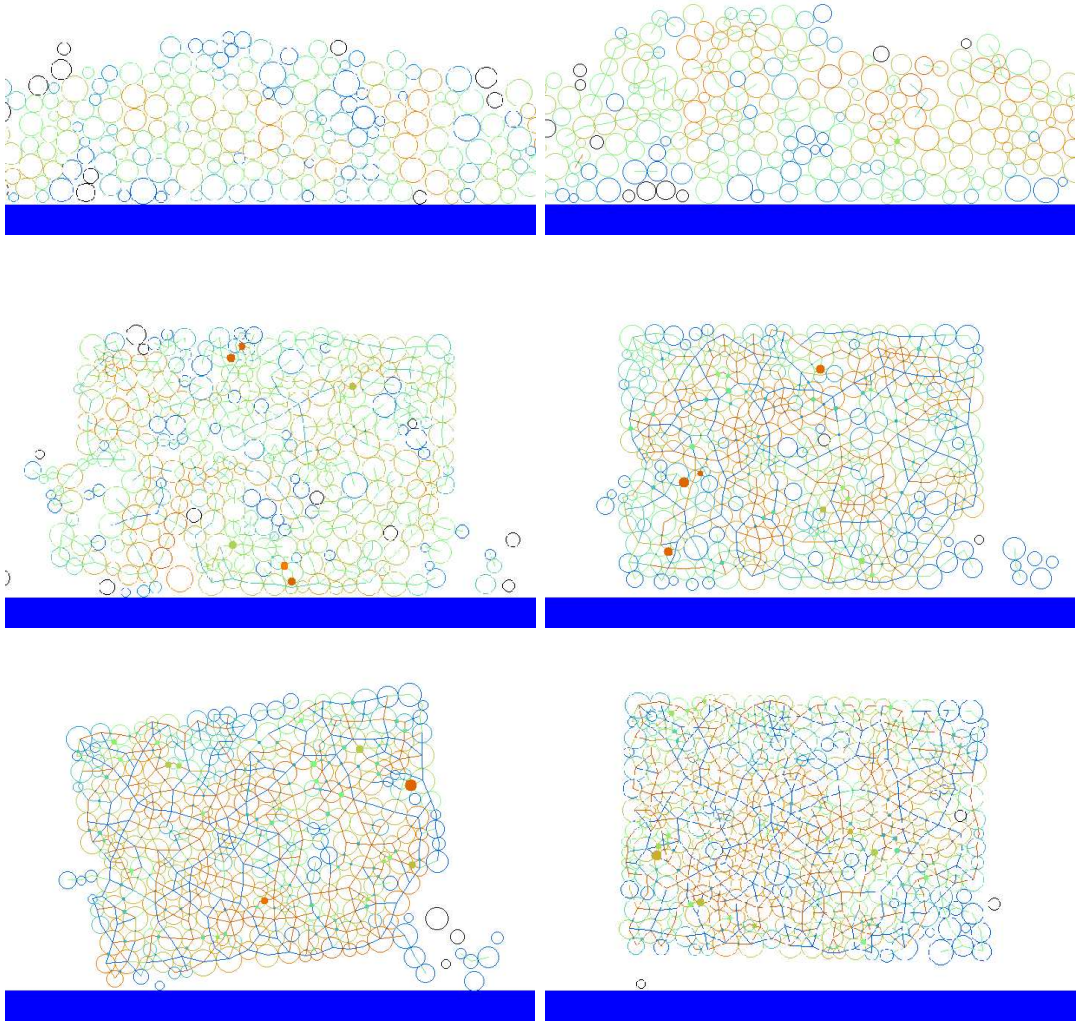

Figure 4. Snapshots after a vibration test with frequency $f = 100\,\mathrm{Hz}$ and amplitude $a = 0.2\,\mathrm{mm}$. The material samples were sintered for $t_s = 10^{-4}$, 0.01, 0.02, 0.05, 0.2, and 1.0 with $p = 10$. The open circles are particles with their colors coding the average stress, blue, green and red correspond to low, medium and large stresses. The lines are the contacts with their colors coding attractive (blue) or repulsive (red) normal forces. The small solid circles denote the tangential forces, with their size proportional to the magnitude of the tangential force.

The sample with the longest sintering time $t_s = 1.0$ is almost perfectly stable even under strong shaking – however, some corner- or boundary particles sometimes still break off, i.e., one has attrition. For shorter sintering time the sample is less stable and breaks into pieces.

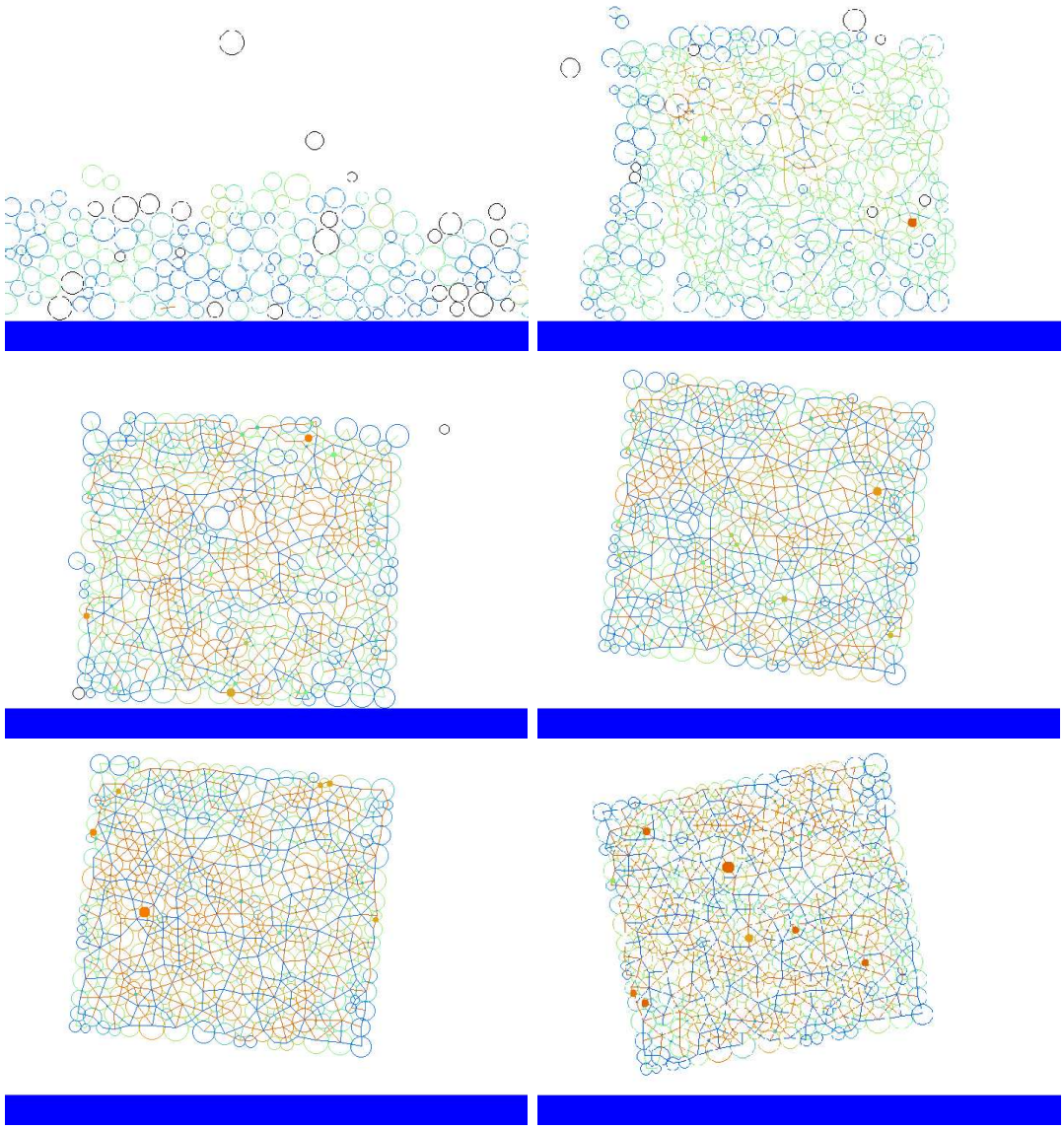

Figure 5. Snapshots after a vibration test. The material samples were sintered for $t_s = 10^{-4}$, 0.01, 0.02, 0.05, 0.2, and 1.0, with $p = 100$. The color coding and meaning of lines/circles is the same as in Fig. 4.

In Fig. 5, the external compression was stronger so that, for the same sintering duration, more stable agglomerates are formed. Breakage and attrition is weaker for larger confining stress.

5. Summary and Conclusion

A discrete model for the sintering of particulate materials was introduced and simple material samples were sintered for different times and confining pressures. Then they were tested with respect to their anisotropic load strength: Longer sintering and stronger

confining pressure systematically increases the density and the strength of the material. With a vibration test, the breakage and attrition behavior was tested. Depending on the sintering duration, either isolated particles, fragments, or a single solid block of material could be produced. Short sintering time and smaller pressure lead to stronger attrition.

The research to be done in the future is an accurate testing of the model via a comparison with experimental data. Since these are only available in three-dimensional systems, the 2D model presented here has to be extended to three dimensions, where "only" more particles are needed. Note that the model presented (without optimization or tuning) increases the amount of computation necessary for each contact by a large factor. The last, still missing ingredients for a realistic model are rolling- and torsion-resistance.

6. Acknowledgements

The author thanks M. Lätzel, J. Tomas, S. Diebels, H. Besserer, K. Manetsberger, J. Müllers, and G. A. D´Addetta for helpful discussions and acknowledge financial support by the Deutsche Forschungsgemeinschaft (DFG), by the DaimlerChrysler research division.

References

[1] A. Jagota, K. R. Mikeska, and R. K. Bordia. *Isotropic constitutive model for sintering particle packings.* Journal of the American Ceramic Society, 73(8):2266–2273, 1990.

[2] A. Jagota and G. W. Scherer. *Viscosities and sintering rates of composite packings of spheres.* Journal of the American Ceramic Society, 78(3):521–528, 1995.

[3] E. A. Olevsky. *Theory of sintering: from discrete to continuum.* Materials Science and Engineering, R23:41–100, 1998.

[4] C. T. Bellehumeur, M. Kontopoulou, and J. Vlachopoulos. *The role of viscoelasticity in polymer sintering.* Rheol. Acta, 37:270–278, 1998.

[5] M. R. Zachariah and M. J. Carrier. *Molecular dynamics computation of gas-phase nanoparticle sintering: A comparison with phenomenological models.* J. Aerosol Science, 30(9):1139–1151, 1999.

[6] H. Riedel and B. Blug. *A comprehensive model for solid state sintering and its application to silicon carbide.* In T.-J. Chuang and J. W. Rudnicki, editors, Multiscale deformation and fracture in materials and structures, the James R. Rice 60th anniversary volume, Solid mechanics and its application - Vol. 84, pages 49–70, Dordrecht, 2001. Kluwer Academic Publishers.

[7] K. Manetsberger, J. Shen, and J. Muellers. *Compensation of Non-Linear Shrinkage of Polymer Materials in Selective Laser Sintering.* In Solid Freeform Fabrication Symposium 2001, (Proceedings), pp. 221–232, 2001.

[8] L. A. Anestiev and L. Froyen. *Model of the primary rearrangement processes at liquid phase sintering and selective laser sintering due to biparticle interactions.* J. Appl. Phys. 86(7):4008–4017, 1999.

[9] T. Kraft, H. Riedel, and O. Rosenfelder. *Compaction and sintering of a ceramic seal: Modeling and experimental response.* Int. J. Powder Metallurgy, 39(6):27–34, 2003.

[10] H. J. Herrmann, J.-P. Hovi, and S. Luding, editors. *Physics of dry granular media - NATO ASI Series E 350*, Dordrecht, 1998. Kluwer Academic Publishers.

[11] D. P. DeLo, R. E. Dutton, and S. L. Semiatin. *A comparison of discrete element model prediction to observation of metal powder consolidation.* Scripta Materialia, 40(10):1103–1109, 1999.

[12] S. Luding, K. Manetsberger, and J. Muellers, *A discrete model for long time sintering*, Journal of the Mechanics and Physics of Solids 53(2), 455-491, 2005.

[13] S. Luding, *A discrete particle-contact model for sintering*, in: Numerical Modeling in Micromechanics via Particle Methods - 2004, Y. Shimizu, R. D. Hart, and P. A. Cundall (eds.), PFC Symposium proceedings, A. A. Balkema, Leiden, 2004 (ISBN 90-5809-679-3), pp. 127-134.

[14] P. Redanz and N. A. Fleck. *The compaction of a random distribution of metal cylinders by the discrete element method.* Acta Materialia, 49:4325–4335, 2001.

[15] A. Jagota and P. R. Dawson. *Simulation of the viscous sintering of 2 particles.* Journal of the American Ceramic Society, 73(1):173–177, 1990.

[16] P. A. Cundall and O. D. L. Strack. *A discrete numerical model for granular assemblies.* Géotechnique, 29(1):47–65, 1979.

[17] C. Thornton and S. J. Antony. *Quasi-static deformation of particulate media.* Phil. Trans. Roy. Soc. A, 1998.

[18] O. R. Walton and R. L. Braun. *Viscosity, granular-temperature, and stress calculations for shearing assemblies of inelastic, frictional disks.* Journal of Rheology, 30(5):949–980, 1986.

[19] S. Luding. *Collisions & contacts between two particles.* In H. J. Herrmann, J.-P. Hovi, and S. Luding, editors, *Physics of dry granular media - NATO ASI Series E350*, page 285, Dordrecht, 1998. Kluwer Academic Publishers.

[20] Jürgen Tomas. *Particle adhesion fundamentals and bulk powder consolidation.* KONA, 18:157–169, 2000.

[21] S. Luding, R. Tykhoniuk, and J. Tomas, *Anisotropic material behavior in dense, cohesive powders*, CET (Chemical Engineering Technology) 26 (12), 1229-1232, 2003.

[22] S. Luding, *Molecular Dynamics Simulations of Granular Materials*, in: The Physics of Granular Media, H. Hinrichsen and D. Wolf, eds., Wiley-VCH, Weinheim, 2004 (ISBN 3-527-40373-6), pp. 299-324.

[23] J. Svoboda, H. Riedel, and H. Zipse. *Equilibrium pore surfaces, sintering stresses and constitutive equations for the intermediate and late stages of sintering – I. Computation of equilibrium surfaces.* Acta metall. mater., 42:435–443, 1994.

[24] H. Riedel, H. Zipse, and J. Svoboda. *Equilibrium pore surfaces, sintering stresses and constitutive equations for the intermediate and late stages of sintering – II. Diffusional densification and creep.* Acta metall. mater., 42:445–452, 1994.